J|A|C|S
ARTICLES
Published on Web 12/17/2004

Trimer Based Polarization as a Multibody Molecular Model. Application to Hydrogen Fluoride

Scott J. Wierzchowski and David A. Kofke*

Contribution from the Department of Chemical and Biological Engineering, University at Buffalo, The State University of New York, Buffalo, New York 14260-4200

Received December 21, 2003; E-mail: kofke@buffalo.edu

Abstract: A molecular modeling approach is introduced as a way to treat multibody (more than two molecules) contributions to the intermolecular potential. There are two key features to the method. First, it employs polarizable electrostatics on the molecules, but converges the charges and fields for only three molecules at a time, taken separately for all trimers (three molecules falling within a cutoff distance) in the system. This feature introduces significant computational savings when applied in Monte Carlo simulation (in comparison to a full *N*-body polarization treatment), as movement of a single molecule does not require re-converging of the polarization of all molecules, and it achieves this without approximations that cause the value of the energy to depend on the history of the simulation. Second, the approach defines the polarization energy in excess of the pairwise contribution, meaning that the trimer energy has subtracted from it the sum of the energies obtained by converging the polarization of each molecule pair in the trimer. This feature is advantageous because it removes the need (often found in polarizable models) to stiffen inappropriately the repulsive part of the pair potential. The polarization contribution is thus a purely three-body potential. The approach is applied to model hydrogen fluoride, which in experiments exhibits unusual properties that have proven difficult to capture well by molecular models. The new HF model is shown to be much more successful than previous modeling efforts in obtaining agreement with a broad range of experimental data (volumetric properties, heat effects, molecular structure, and vapor−liquid equilibria).

Introduction

Advances in algorithms and in computing hardware have progressed the field of molecular simulation greatly in the past decade.[1] The calculation of thermophysical properties for even very complex molecular models is almost a routine task, given the expertise to select and apply the appropriate techniques. Now the quality of the molecular model is the crucial factor barring the routine application of molecular simulation to the quantitative calculation (or prediction) of the behavior of real systems. It is not yet possible to base a simulation routinely on an ab initio treatment of molecular interactions, so molecular simulations must rely on an approximate treatment of the intermolecular potential. Such models ultimately must be fit to experimental data, although attempts are being made to develop models using ab initio data to varying degrees for this purpose. Several efforts have been made (and are ongoing) to develop transferable potential models, capable of providing predictions about new systems using force fields developed for other systems that have the same functional groups.[2−7] The primary element of most models is an interatomic pairwise potential energy, consisting of van der Waals and Coulombic interactions, and perhaps others. It has long been known[8−11] that pairwise-additive potentials are generally inadequate if one is interested in quantitative agreement with experimental data over a wide range of thermodynamic states, and extensions of these models are made to incorporate the effects of multibody interactions. Polarizable models currently are a popular means to incorporate these features.[8,12−19] In such models electrostatic sites (charges or point multipoles) are placed on the molecules, and the presence of electric fields originating from charges on surrounding molecules polarizes these sites, giving rise to a new electrostatic charge distribution on the molecule.[20] This distribution creates its own electric field that influences the surrounding

(1) Frenkel, D.; Smit, B. *Understanding Molecular Simulation: From Algorithms to Applications*, 2nd ed.; Academic Press: San Diego, 2002.
(2) Siepmann, J. I. *NIST Special Publication* **2001**, *975*, 110−112.
(3) de Pablo, J. J.; Escobedo, F. A. *Aiche. J.* **2002**, *48*, 2716−2721.
(4) Jorgensen, W. L. *J. Am. Chem. Soc.* **1981**, *103*, 335−340.
(5) Jorgensen, W. L. *J. Am. Chem. Soc.* **1981**, *103*, 341−345.
(6) Jalaie, M.; Lipkowitz, K. B. *Rev. Comput. Chem.* **2000**, *14*, 441−486.
(7) Jorgensen, W. L.; Maxwell, D. S.; TiradoRives, J. *J. Am. Chem. Soc.* **1996**, *118*, 11225−11236.
(8) Chialvo, A. A.; Cummings, P. T. *J. Chem. Phys.* **1996**, *105*, 8274−8281.
(9) Kress, J. W.; Kozak, J. J. *J. Chem. Phys.* **1976**, *64*, 1706−1719.
(10) Dang, L. X. *J. Phys. Chem. B* **1998**, *102*, 620−624.
(11) Gonzalez, M. A.; Enciso, E.; Bermejo, F. J.; Bee, M. *J. Chem. Phys.* **1999**, *110*, 8045−8059.
(12) Svishchev, I. M.; Kusalik, P. G.; Wang, J.; Boyd, R. J. *J. Chem. Phys.* **1996**, *105*, 4742−4750.
(13) Jedlovszky, P.; Vallauri, R. *J. Chem. Phys.* **2001**, *115*, 3750−3762.
(14) Jedlovszky, P.; Vallauri, R. *J. Chem. Phys.* **1997**, *107*, 10166−10176.
(15) Banks, J. L.; Kaminski, G. A.; Zhou, R. H.; Mainz, D. T.; Berne, B. J.; Friesner, R. A. *J. Chem. Phys.* **1999**, *110*, 741−754.
(16) Stern, H. A.; Kaminski, G. A.; Banks, J. L.; Zhou, R. H.; Berne, B. J.; Friesner, R. A. *J. Phys. Chem. B* **1999**, *103*, 4730−4737.
(17) Stern, H. A.; Rittner, F.; Berne, B. J.; Friesner, R. A. *J. Chem. Phys.* **2001**, *115*, 2237−2251.
(18) Dykstra, C. E. *Adv. Chem. Phys.* **2003**, *126*, 1−40.
(19) Kaminski, G. A.; Friesner, R. A.; Zhou, R. *J. Comput. Chem.* **2003**, *24*, 267−276.
(20) Bottcher, C. J. F. *Theory of Electric Polarization, Vol. 1: Dielectrics in Static Fields*; Elsevier: Amsterdam, 1973.

10.1021/ja031877b CCC: $30.25 © 2005 American Chemical Society

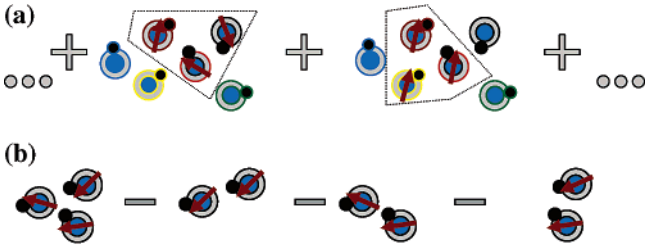

Figure 1. Illustration of the principal features of the 3-body component of the TBP potential. Circles are cartoon HF molecules, and arrows are illustrations of the dipole moment on each. (a) polarization is converged separately for each set of three neighboring molecules, and energy includes a sum of all such contributions; (b) polarization is converged for each pair of molecules, and these 2-body interactions are subtracted from each 3-body contribution.

molecules, changing their charges and the resulting field, and the whole assemblage of fixed and polarizable charges must be converged to a self-consistent distribution.

There are at least two drawbacks to the use of polarizable models for treating multibody interactions. First is the computational cost. Movement of any molecule in the system of N molecules affects the charges on all other molecules, introducing an $O(N^2)$ calculation to update the energy for any such perturbation. This issue does not complicate molecular dynamics simulation, because all atoms are moved in every step, and the $O(N^2)$ calculation is required regardless. However, this feature significantly complicates the application of Monte Carlo (MC) methods to the study of polarizable models. This outcome is very unfortunate, as Monte Carlo encompasses many important and otherwise advantageous simulation methods.[1] Attempts to surmount this problem are being made,[19,21,22] but these remedies have their own costs. In one case, an approximation is introduced that leads the potential to become ill-defined, in the sense that the energy ascribed to a configuration depends (to a small degree) on the recent history of the simulation. The second drawback of polarizable models receives less attention. Polarization contributes substantially to the pair interaction, particularly at short range, and the attraction so induced necessitates buttressing of the repulsion between atom pairs. The result is a considerably stiffer potential than is appropriate, contributing to a degradation of the quality of the model.

In the present work, we present a polarization-based approach to multibody interactions that addresses both of the concerns raised above. There are two important features to the treatment, both connected to a 3-body formulation of the polarization, and they are illustrated in Figure 1. First, the potential energy is based on convergence of the electric field for three molecules at a time (Figure 1a). As a consequence each molecule in a given configuration does not possess a well-defined dipole moment (for example), but nevertheless the energy of the configuration is well defined and independent of the history of the simulation. This modeling feature lowers the computational cost of the potential model when applied in MC simulation. Second, the 2-body polarization effects are removed from the model—they are simply subtracted out, so the polarization model is truly a 3-body potential (Figure 1b). This feature allows for a certain transferability: the polarization effects can be added to a pure 2-body model without concern that it impacts the 2-body form. The notion of a pure 3-body interaction is a well-established idea, and the explicit subtraction of 2-body interactions from a 3-body energy is found in other multibody potential models. The novel feature here is the application of this approach in the context of polarizable models where the norm is to formulate pair interactions in conjunction with the N-body polarizable interactions. An important advantage of the proposed approach is that it permits the use of a softer repulsion in the 2-body part of the model, because there is no issue with having inappropriately large attractions induced between pairs in close proximity.

We demonstrate this modeling approach in application to hydrogen fluoride (HF). HF is of great importance technologically[23] and it is very interesting scientifically, inasmuch as it presents a good prototype for understanding the nature and effects of hydrogen bonding.[24−28] Accordingly, HF has been the subject of intense theoretical study using ab initio computational chemistry, and many theoretically or empirically based molecular models have been proposed for it.[14,29−37] All such models have failed to describe its bulk-phase properties—some features have not even been captured qualitatively. HF exhibits many anomalous properties attributable to the effects of strong hydrogen-bonded association or clustering, particularly in the vapor phase. These behaviors include very large heat-capacity peaks in the superheated vapor,[38,39] a maximum in the heat of vaporization,[40−44] very low surface tension,[45] and a highly nonideal vapor-phase equation of state.[38,39]

The aggressive and toxic nature of HF hampers its study by experiment. For example, measurements of heat effects of the superheated vapor has been limited to low-pressure regions.[38] Experimental observations of the compressibility factor of HF indicate that association can persist well into the superheated vapor, so it would be valuable to have a more comprehensive set of data regarding its properties at more difficult conditions. Molecular modeling can aid in filling gaps in the experimental data. If an interaction model is able to reproduce the available

(21) Predota, M.; Cummings, P. T.; Chialvo, A. A. *Mol. Phys.* **2001**, *99*, 349−354.
(22) Mahoney, M. W.; Jorgensen, W. L. *J. Chem. Phys.* **2001**, *114*, 9337−9349.
(23) Ullmann, F. *Ullmann's Encyclopedia of Industrial Chemistry*, 6th ed.; Wiley: New York, 2000.
(24) Redington, R. L. *J. Chem. Phys.* **1981**, *75*, 4417−4421.
(25) Redington, R. L. *J. Phys. Chem.* **1982**, *86*, 552−560.
(26) Quack, M.; Stohner, J.; Suhm, M. A. *J. Mol. Struct.* **2001**, *599*, 381−425.
(27) Klopper, W.; Quack, M.; Suhm, M. A. *J. Chem. Phys.* **1998**, *108*, 10096−10115.
(28) Suhm, M. A. *Ber. Bunsen-Ges. Phys. Chem.* **1995**, *99*, 1159−1167.
(29) Klein, M. L.; McDonald, I. R.; O'Shea, S. F. *J. Chem. Phys.* **1978**, *69*, 63−66.
(30) Barton, A. E.; Howard, B. J. *Faraday Discuss. Chem. Soc.* **1982**, *73*, 45−62.
(31) Honda, K. *J. Chem. Phys.* **2002**, *117*, 3558−3569.
(32) Honda, K.; Kitaura, K.; Nishimoto, K. *B Chem. Soc. Jpn.* **1992**, *65*, 3122−3134.
(33) Cournoyer, M. E.; Jorgensen, W. L. *Mol. Phys.* **1984**, *51*, 119−132.
(34) Kreitmeir, M.; Bertagnolli, H.; Mortensen, J. J.; Parrinello, M. *J. Chem. Phys.* **2003**, *118*, 3639−3645.
(35) Della Valle, R. G.; Gazzillo, D. *Phys. Rev. B* **1999**, *59*, 13699−13706.
(36) Wierzchowski, S. J.; Kofke, D. A. *J. Chem. Phys.* **2003**, *119*, 6092−6099.
(37) Wierzchowski, S. J.; Kofke, D. A.; Gao, J. *J. Chem. Phys.* **2003**, *119*, 7365−7371.
(38) Franck, E. U.; Meyer, F. *Z. Elektrochem.* **1959**, *63*, 571−582.
(39) Vanderzee, C. E.; Rodenburg, W. W. *J. Chem. Thermodyn.* **1970**, *2*, 461−478.
(40) Hu, J.-H.; White, D.; Johnston, H. L. *J. Am. Chem. Soc.* **1953**, *75*, 1232−1236.
(41) Yabroff, R. M.; Smith, J. C.; Lightcap, E. H. *J. Chem. Eng. Data* **1964**, *9*, 178−182.
(42) Fredenhagen, K.; Butzke, U. *Z. Anorg. Allgem. Chem.* **1934**, *218*, 165−168.
(43) Fredenhagen, K. *Z. Anorg. Allgem. Chem.* **1933**, *210*, 210−224.
(44) Simons, J. H.; Bouknight, J. W. *J. Am. Chem. Soc.* **1933**, *55*, 1458−1460.
(45) Simons, J. H.; Bouknight, J. W. *J. Am. Chem. Soc.* **1932**, *54*, 129−137.

experimental properties of HF, then one gains confidence in extrapolating the model to other properties and state conditions. Moreover, development of robust modeling methods for this (arguably) worst-case substance can lead to advances in models applied to other important systems, such as water, for which modeling is still unable to give quantitative agreement with bulk-phase experimental behavior over broad state conditions.[8,46]

This paper is organized as follows. In the next section, we describe the trimer-based polarization (TBP) approach, and present parameters for a HF model based upon it. The subsequent section explains how we examine via molecular simulation four regions on the HF phase diagram: liquid, supercritical fluid, vapor−liquid coexistence, and superheated vapor. Then we present and analyze the results, and finish with a summary.

Model

In the proposed model, the total configurational potential energy U for N molecules is the sum of one-, two-, and three-body terms, plus an Ewald treatment of long-range electrostatics

$$U^{\text{tot}} = \sum_i U_i + \sum_i \sum_{j>i} U_{ij} + \sum_i \sum_{j>i} \sum_{k>j} U_{ijk} + U^{\text{Ewald}} \quad (1)$$

The three-body term is key to this approach, so we consider it in detail first.

The electrostatic features of each molecule are described through N^{sites} fixed charges q_{ia} plus an induced dipole that appears in response to the electric field created by its neighbors. The total potential is defined such that the induced dipole contributes only via the three-body terms. The three-body contribution, U_{ijk}, to the total energy is given by the induced electrostatic energy of the three molecules, computed in excess of the induced electrostatics when each of the three is considered a pair at a time. Specifically

$$U_{ijk} = \tilde{U}_{ijk} - \tilde{U}_{ij} - \tilde{U}_{ik} - \tilde{U}_{jk} \quad (2)$$

where the tildes indicate the converged induction energies for the trimer

$$\tilde{U}_{ijk} = -\frac{1}{2}(\mu_i^{(ijk)}\mathbf{E}_i^{(ijk)} + \mu_j^{(ijk)}\mathbf{E}_j^{(ijk)} + \mu_k^{(ijk)}\mathbf{E}_k^{(ijk)}) \quad (3)$$

and each of the three pairs

$$\tilde{U}_{ij} = -\frac{1}{2}(\mu_i^{(ij)}\mathbf{E}_i^{(ij)} + \mu_j^{(ij)}\mathbf{E}_j^{(ij)}) \quad (4)$$

(with $\tilde{U}_{jk}$ and $\tilde{U}_{ik}$ defined similarly). In eqs 3 and 4, the appropriate electric field due to the permanent charges, $\mathbf{E}$, and induced dipole moments, μ, define each energy contribution. The electric field from neighboring molecules arises in the form of

$$\mathbf{E}_i^{(ij)} = \frac{1}{4\pi\epsilon_o}\sum_{a=1}^{N^{\text{sites}}} \frac{\mathbf{r}_{ija}q_{ja}}{r_{ija}^3} \quad (5)$$

for a two molecule interaction (j on i) and

$$\mathbf{E}_i^{(ijk)} = \frac{1}{4\pi\epsilon_o}\sum_{a=1}^{N^{\text{sites}}} \left(\frac{\mathbf{r}_{ija}q_{ja}}{r_{ija}^3} + \frac{\mathbf{r}_{ika}q_{ka}}{r_{ika}^3}\right) \quad (6)$$

for a three molecule interaction (j and k on i); $\mathbf{E}_j$ and $\mathbf{E}_k$ can found by simply changing appropriate subscripts.

After the electric field is defined, the matrix $\boldsymbol{T}^{(ij)}$ is calculated

$$\boldsymbol{T}^{(ij)} = \frac{1}{r_{ij}^3}\left(\frac{3\mathbf{r}_{ij}\mathbf{r}_{ij}}{r_{ij}^2} - \boldsymbol{I}\right) \quad (7)$$

where $\boldsymbol{I}$ is the identity matrix. The induced dipoles, μ_i, μ_j, and μ_k, must be calculated for three two-molecule interactions (molecule i with molecule j, i with k, and j with k) and a three molecule interaction, molecules i, j, and k. This is done separately for each combination of three molecules obtainable from the N molecules in the system. In practice, we apply a cutoff to the interaction, such that if any two molecules of the three are separated by a distance greater than a cutoff r_c, the three-body contribution of the trimer is zero. Attention was given to ensure that all molecules reside within a single periodic image of one another, as an unambiguous group of three molecules.

The two-molecule interaction, molecule i with molecule j, yields μ_i and μ_j via

$$\mu_i^{(ij)} = \alpha(\mathbf{E}_i^{(ij)} + \boldsymbol{T}^{(ji)}\cdot\mu_j^{(ij)}) \quad (8)$$

$$\mu_j^{(ij)} = \alpha(\mathbf{E}_j^{(ij)} + \boldsymbol{T}^{(ji)}\cdot\mu_i^{(ij)}) \quad (9)$$

where α is the scalar molecular polarizability. For the immediate calculations, we choose to work with a scalar polarizability but application of an anisotropic polarizability is a proposition that is conveniently incorporated into the present methodology. From these two equations, we can derive an independent equation for $\mu_i^{(ij)}$

$$\mu_i^{(ij)} = \alpha(\boldsymbol{I} - \alpha\boldsymbol{T}^{(ij)}\boldsymbol{T}^{(ji)})^{-1}(\mathbf{E}_i^{(ij)} + \alpha\boldsymbol{T}^{(ji)}\mathbf{E}_j^{(ij)}) \quad (10)$$

We now can solve for $\mu_j^{(ij)}$ by using eq 9. The same procedure is repeated for the other two pairs. The energy contributions $\tilde{U}_{ij}$, $\tilde{U}_{ik}$, and $\tilde{U}_{jk}$ can then be calculated via eq 4.

To evaluate the energy contribution $\tilde{U}_{ijk}$, we follow a similar procedure. We must calculate $\mu_i^{(ijk)}$, $\mu_j^{(ijk)}$, and $\mu_k^{(ijk)}$ for a three molecule system

$$\mu_i^{(ijk)} = \alpha(\mathbf{E}_i^{(ijk)} + \boldsymbol{T}^{(ji)}\mu_j^{(ijk)} + \boldsymbol{T}^{(ji)}\mu_k^{(ijk)}) \quad (11)$$

with similar equations for $\mu_j^{(ijk)}$ and $\mu_k^{(ijk)}$. Because we involve only three molecules, these coupled formulas for the induced dipole moments can be solved explicitly

$$\mu_i^{(ijk)} = \alpha(\boldsymbol{I} - \alpha^2(\boldsymbol{DAB} + \boldsymbol{T}^{(ik)}\boldsymbol{T}^{(ki)}))^{-1} \times (\mathbf{E}_i^{(ijk)} + \alpha(\boldsymbol{DAC} + \boldsymbol{T}^{(ik)}\mathbf{E}_k^{(ijk)})) \quad (12)$$

$$\mu_j^{(ijk)} = \alpha(\boldsymbol{AC} + \boldsymbol{AB}\mu_i^{(ijk)}) \quad (13)$$

and

$$\mu_k^{(ijk)} = \alpha(\mathbf{E}_k^{(ijk)} + \boldsymbol{T}^{(ki)}\mu_i^{(ijk)} + \boldsymbol{T}^{(kj)}\mu_j^{(ijk)}) \quad (14)$$

where

(46) Chialvo, A. A.; Yezdimer, E.; Driesner, T.; Cummings, P. T.; Simonson, J. M. *Chem. Phys.* **2000**, *258*, 109−120.

$$\boldsymbol{A} = (\boldsymbol{I} - \alpha^2 \boldsymbol{T}^{(jk)}\boldsymbol{T}^{(kj)})^{-1} \quad (15)$$

$$\boldsymbol{B} = \boldsymbol{T}^{(ji)} + \alpha \boldsymbol{T}^{(jk)}\boldsymbol{T}^{(ki)} \quad (16)$$

$$\boldsymbol{C} = \mathbf{E}_j^{(ijk)} + \alpha \boldsymbol{T}^{(jk)}\mathbf{E}_k^{(ijk)} \quad (17)$$

and

$$\boldsymbol{D} = \boldsymbol{T}^{(ij)} + \alpha \boldsymbol{T}^{(ik)}\boldsymbol{T}^{(kj)} \quad (18)$$

$\tilde{U}_{ijk}$ can be then calculated from eq 3 for the three molecule system.

Subtraction of the two-body terms from the 3-body polarization energy in eq 2 causes the polarization contribution to be a true 3-body effect. If any of the molecules are far from the other two, the polarization contribution vanishes. An appealing feature of this formulation is that the 3-body contribution can be added on to any 2-body potential without concern that it will alter the original pair interaction.

For modeling of HF in this work, the TBP 3-body interaction is added to a classical 2-body potential surface consisting of a Hartree−Fock dispersion (HFD) term,[47] plus Coulombic charge−charge interactions. The HFD contribution is defined

$$U_{ij}^{\mathrm{vdW}} = U_{ij}^{\mathrm{HFD}} = A \exp(-\tau^{\mathrm{HFD}} r_{ij}) + (C_6 r_{ij}^{-6} + C_8 r_{ij}^{-8} + C_{10} r_{ij}^{-10}) F(r_{ij}) \quad (19)$$

with

$$F(r_{ij}) = \begin{cases} \exp\left(-\left(\dfrac{D}{r_{ij}} - 1\right)^2\right) & r_{ij} < D \\ 1 & r_{ij} \geq D \end{cases} \quad (20)$$

where τ^{HFD}, A, C_6, C_8, C_{10}, and D are adjustable parameters. The charge−charge interaction is of the standard form

$$U_{ij}^{qq} = \frac{1}{4\pi\epsilon} \sum_{i \in a}^{N^{\mathrm{sites}}} \sum_{j \in b}^{N^{\mathrm{sites}}} \frac{q_{ia} q_{jb}}{r_{ijab}} \quad (21)$$

We apply the standard Ewald summation to account for the long-range electrostatic contributions, using tinfoil boundary conditions.[48,49] The Ewald contribution considers only the fixed charges, and does not include or affect the polarizable charges in any way.

Finally, we employ a flexible model for the HF molecule, allowing bond stretching governed by a Morse-type intramolecular potential

$$U_i^M = D_e[1 - \exp(-\tau^M(r_{ab} - r_{eq}))]^2 \quad (22)$$

where D_e is the monomer dissociation energy, τ^M is an effective range parameter and r_{eq} is the equilibrium bond length. To limit the ability of the monomer to stretch excessively, an additional term is applied when the separation exceeds a value $r_{ab}^{\max}$

$$U_i = U_i^M + \epsilon^M (U_i^M / U_i^{\max})^8 \quad (23)$$

where $U_i^{\max}$ is the value of U_i^M at $r_{ab}^{\max}$, $U_i \cong U_i^M$ when $U_i^M \ll U_i^{\max}$, and $U_i \gg U_i^{\max}$ when $r_{ab} \gg r_{ab}^{\max}$; also $\epsilon^M = 1$ kcal/mol to fix the units of the added term.

The parameters for the model were selected as follows. The point charges were chosen to approximate the experimental quadrupole[50,51] (2.36 B) and dipole moments[50,52,53] (1.83 D). Here we end up slightly exaggerating these values to 2.38 and 1.86, respectively. The point charges were arranged collinearly with $-2q$ displaced 0.171 Å and q displaced 0.930 Å from the fluorine-centered charge q (where q equals 0.66 e), both displacements toward the hydrogen atom. The van der Waals parameters, A, τ^{HFD}, C_6, and C_8, C_{10}, were fit to experimental densities (with primary adjustment to C_8 and C_{10} as other values can be compared to previous published van der Waals parameters) at 300 K, 2 atm and 473 K, and 77 atm, yielding A = 169 300 kcal/mol, τ^{HFD} = 4.136 Å^{-1}, C_6 = 265 Å^6 kcal/mol, C_8 = 1700 Å^8 kcal/mol, C_{10} = 34000 Å^{10} kcal/mol, and D = 4.7 Å (taken from ref 54). The scalar polarizability, α, was set to experimental value[50] of 0.83 Å^3. The intramolecular energy was defined by: D_e, the dissociation energy, equal to 140.0 kcal/mol; τ^M = 2.2185 Å^{-1} and r_{eq}, = 0.930 Å (comparable to what is suggested by Pfleiderer et al.[55]). The parameters τ^M and D_e were taken from Della Valle et al.[35] The value of $r_{ab}^{\max}$ was chosen to be 0.983 Å, which is near the experimentally determined value[56] for the gas-phase hexamer bond length of 0.973 Å. It should be noted that all aspects of the model and simulations of it deal only with classical motion of the nuclei and omit the zero-point energy. The well depth of the potential is 5.1 kcal/mol, which can be compared to the true pair values of 4.6 kcal/mol without the zero-point correction, or 3.1 kcal/mol with it.[57]

A less rigorous approach to define a three-body energy is to employ an unconverged induced dipole moment as

$$\mu_i^{ind} = \alpha \mathbf{E}_i^q \quad (24)$$

Application of this induction model into the three-body formulation defines a different potential model, TBP*, which removes a number of matrix operations. It is of interest to see whether TBP* will produce results similar to the TBP model, similar in fashion to approximate all-molecule polarization approaches shown recently.[19,58] In addition, the behavior of the TBP pair potential by itself (without any 3-body contributions) is of interest; we denote this model TBP-2B. As a result three models are simulated for HF, giving a sense of how the formulations change the properties.

Computational Methods

We examine the proposed modeling scheme as applied to HF, considering four types of properties: equation of state; heat effects; vapor−liquid coexistence; and molecular structure via the radial

(47) Maitland, G. C.; Rigby, R.; Smith, E. B.; Wakeham, W. A. *Intermolecular Forces. Their Origin and Determination*; Clarendon Press: Oxford, 1981; Vol. 3.
(48) Nymand, T. M.; Linse, P. *J. Chem. Phys.* **2000**, *112*, 6152−6160.
(49) Heyes, D. M. *Phys. Rev. B* **1994**, *49*, 755−764.
(50) Gray, C. G.; Gubbins, K. E. *Theory of Molecular Fluids*; Clarendon Press: Oxford, 1984; Vol. Volume 1: Fundamentals.
(51) De Leeuw, F. H.; Dymanus, A. *J. Mol. Spectrosc.* **1973**, *48*, 427−445.
(52) Nelson, R. D., Jr.; Lide, D. R.; Maryott, A. A. *Nat'l Stand. Ref. Data Ser. (U. S., Nat'l Bur. Stand.)* **1967**, *No. 10*, 49 pp.
(53) Munter, J. S.; Klemperer, W. *J. Chem. Phys.* **1970**, *52*, 6033−6037.
(54) Klein, M. L.; Mcdonald, I. R.; Righini, R. *J. Chem. Phys.* **1979**, *71*, 3673−3682.
(55) Pfleiderer, T.; Waldner, I.; Bertagnolli, H.; Todheide, K.; Fischer, H. E. *J. Chem. Phys.* **2000**, *113*, 3690−3696.
(56) Janzen, J.; Bartell, L. S. *J. Chem. Phys.* **1969**, *50*, 3611−3618.
(57) Quack, M.; Suhm, M. A. In *Conceptual Perspectives in Quantum Chemistry*; Calais, J.-L., Kryachko, E. S., Eds.; Kluwer: Dordrecht, 1997; Vol. III, pp 415−463.
(58) Palmo, K.; Krimm, S. *Chem. Phys. Lett.* **2004**, *395*, 133−137.

Table 1. State Conditions for Study of RDFs of HF[a]

label	T (K)	P (atm)	ρ (g/cm^3)	TBP ρ (g/cm^3)	TBP-2B ρ (g/cm^3)	JVP[b] ρ (g/cm^3)	CJ84[b] ρ (g/cm^3)	error (%) TBP; JVP; CJ84
I	300	2	0.962	1.033(5)	1.134(2)	0.924(28)	0.971(58)	+7; −4; +1
II	373	12	0.796	0.837(6)	0.855(10)	0.774(39)	0.633(41)	+4; −3; −20
III	473	314	0.796	0.723(5)	0.637(5)	0.584(50)	0.579(39)	−9; −27; −27
IV	473	164	0.647	0.589(8)	0.289(6)	0.334(47)	0.423(41)	−13; −48; −35
V	473	83	0.398	0.136(3)	0.071(1)	0.081(70)	0.091(16)	−66; −80; −77
VI	473	77	0.236	0.109(2)	0.063(1)	0.068(5)	0.081(7)	−54; −71; −66

[a] First column is a label used to reference each state in the test. Next three columns are experimental[62,64,69] values of the temperature, pressure, and density, respectively. Next four columns are, respectively, densities for the TBP model (determined here), TBP-2B pair potential, the Jedlovzsky−Vallauri polarizable model[14] and the Cournoyer−Jorgensen model,[65] both as reported in ref 64; numbers in parentheses indicate the 67% confidence limit of the last digits of the reported value. Last column is the percent error of the TBP/JVP/CJ84 simulation densities, taken with respect to the experimental value. States from experiment are indicated by × symbols in Figure 2. [b] As given in ref 64.

distribution function (RDF) and vapor-phase clustering statistics. In all cases we compare the simulation results to available experimental data. We outline here the methods used for our simulations.

Gibbs ensemble (GE) Monte Carlo[59] was used to calculate three vapor−liquid coexistence properties, namely the coexistence densities, the vapor pressure, and the heat of vaporization. Simulations were conducted from 280 to 360 K at 20 K intervals and then to 440 K in 10 K intervals. Each system comprised $N = 500$ molecules distributed between the vapor and liquid phases. The MC trials consisted of (and were performed with relative frequency indicated in parentheses) intramolecular bond stretching (N/3), particle transfers between phases (N, but slightly more frequent at lower temperature), volume exchanges (3), molecule rotations (N), and molecule displacements (N). The molecule displacement and molecule rotation were adjusted to a 40% acceptance rate. The simulations were conducted over more than 5×10^4 cycles (a cycle is N MC trials), with longer simulation lengths applied at higher temperature. Simulation block averages for the density, molar energy and volume differences (ΔU^{vl}, ΔV^{vl}) between phases were taken every 1000 cycles. The vapor pressure, P^{sat}, was calculated by methodologies described by Harismiadis et al.[60] for blocks of at least 5000 cycles. The heat of vaporization, ΔH^{vap}, was determined by

$$\Delta H^{vap} = \Delta U^{vl} + P^{sat}\Delta V^{vl} \tag{25}$$

An alternative to calculating heats of vaporization was also explored by applying the (exact) Clapeyron relation

$$\frac{\partial \ln P^{sat}}{\partial \beta} = \frac{\Delta H^{vap}}{\beta P \Delta V} \tag{26}$$

using a finite difference method to get the slope of the vapor pressure; the latter approach did not produce higher-quality results, so the data here are given via eq 25.

Experimental RDFs are available from Pfleiderer et al.[55] for comparison to distributions measured in simulation. The measured RDFs are a combination of the distributions for the different atom pairs

$$g_{avg} = 0.4966 g_{FH} + 0.2104 g_{FF} + 0.2930 g_{HH} \tag{27}$$

where g_{ij} is the intramolecular RDF for the $i-j$ atomic species. Appropriate comparison of RDFs to experiment should ensure that the simulation matches the experimental density rather than the pressure, so canonical-ensemble (*NVT*) simulation was applied for this purpose. To check the degree of consistency of these calculations with experiment, we additionally performed isothermal−isobaric (*NPT*) simulations at the experimental pressure to see how well the simulation density matches experiment. The states examined here have been previously been studied by us and others for other potential models, and they are summarized in Table 1. Each state is given a label (I through VI) there to facilitate discussion of the results.

The RDF and density calculations were conducted for 1×10^5 cycles. For the *NVT* simulations, MC trials were performed for intramolecular bond stretching (N), molecular rotations ($2N$), and molecular displacements ($2N$). When averaging the RDFs, a sample was taken every 25 cycles. The *NPT* ensemble consisted of the same frequencies with addition of a volume move (1). Block averages for the densities were taken every 1000 cycles.

The superheated vapor was analyzed via *NPT* molecular simulations to measure heat capacities, cluster distributions, enthalpies and densities. Association bias moves[61] were introduced for the vapor phase simulations. Four isobars were examined (over temperature ranges (K) indicated in parentheses) 0.553 (292−312), 1.000 (303−319), 2.722 (328−350), and 3.997 atm (346−368 K). For isobars of 0.553 and 1.000 atm, experimental densities and heat capacities are available for comparison. The simulation heat capacities, C_p, were calculated through both enthalpy fluctuations (for a single simulation) and a finite difference estimate of the enthalpy derivative (across simulations at different temperatures), with comparable results. The cluster distribution was calculated by defining a hydrogen bond when an H atom resides within 2.0 Å of an F atom. The algorithm was able to detect both linear and ring oligomers. A difficulty arises when branching in the hydrogen bonding occurs (more than one H atom within 2.0 Å of an F atom). The occurrence is rare for the TBP potential model and is resolved by only counting a single hydrogen bond when multiple bonds arise.

Results and Discussion

Vapor−Liquid Coexistence. Vapor−liquid coexistence properties are presented in Figures 2−5, where results from GE calculations for the TBP and TBP* models along with the TBP-2B pair potential are compared to experiment and to simulation data reported in the literature for other HF models. Figure 2 shows the full temperature−density coexistence diagram, and in Figure 3 the vapor-phase densities are shown in an expanded plot. The TBP model produces coexistence densities that improve agreement with experiment, exceeding the quality of the data from previous modeling efforts. We have not performed the finite-size scaling analysis needed to obtain an accurate characterization of the critical properties, but it appears that the critical temperature of the model will not be far from the experimental value (461 K),[62] within 20−25 K as seen in Figure 3. This outcome compares very favorably with previous modeling efforts, which typically have found the critical temperature as low as half the experimental value. Previous models often significantly overestimate[36,63] or underestimate the

(59) Panagiotopoulos, A. Z. *Mol. Phys.* **1987**, *61*, 813−826.
(60) Harismiadis, V. I.; Vorholz, J.; Panagiotopoulos, A. Z. *J. Chem. Phys.* **1996**, *105*, 8469−8470.
(61) Wierzchowski, S.; Kofke, D. A. *J. Chem. Phys.* **2001**, *114*, 8752−8762.
(62) Franck, E. U.; Spalthoff, W. *Z. Elektrochem.* **1957**, *61*, 348−357.
(63) Visco, D. P.; Kofke, D. A. *J. Chem. Phys.* **1998**, *109*, 4015−4027.

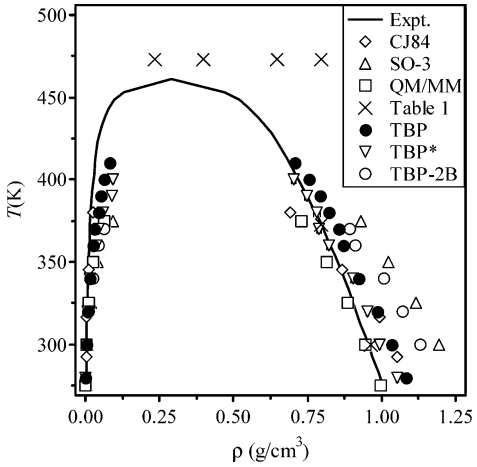

Figure 2. Vapor−liquid coexistence density as calculated from Gibbs ensemble (GE) simulations for the TBP, TBP*, and TBP-2B model and compared to experiment[39,43,45,62,77] (solid line). Also shown are results for the empirical Cournoyer-Jorgensen model (CJ84),[63,65] a quantum-mechanically derived model (SO-3),[27,36] and a recently studied QM/MM based model.[37] Crosses (×) indicate state points of Table 1.

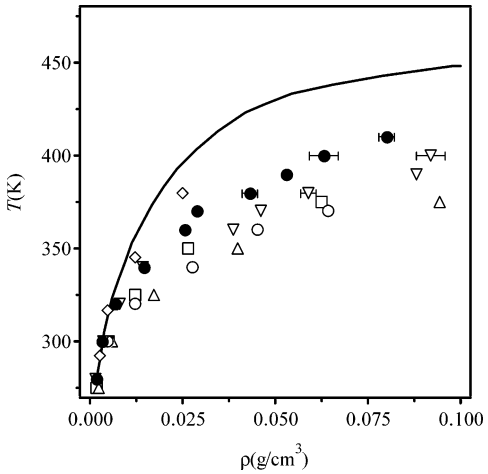

Figure 3. Expanded view of Figure 2, focusing on the vapor-phase densities.

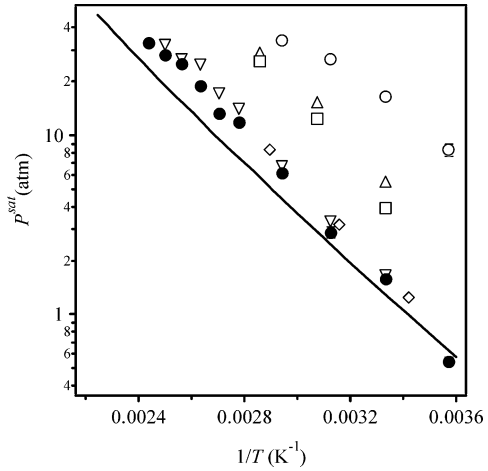

Figure 4. Vapor pressure, P^{sat}, as calculated from GE simulations (circles) through Harismiadis et al. methodology[60] and compared to experiment[39,43,77] (solid line) and models of Figure 2. Symbols are as in Figure 2.

liquid densities.[64] The TBP model overestimates the liquid densities albeit only by 5−7% over the temperature range. The Cournoyer−Jorgensen model[65] and a recently proposed QM/MM approach[37] are the better performers with respect to the densities at lower temperatures, but both are significantly low in estimating the critical temperature. The TBP* model coexistence density is consistently inside the phase envelope of the TBP, revealing only a slight difference in the less rigorous treatment of the polarization. Throughout we present properties for the TBP* but overall behavior is always in accord with the TBP model, and we reserve comments for later. The most pronounced difference in the two approaches is in the TBP* critical point being 5−10 K lower than the TBP model. The TBP-2B pair potential shows liquid coexistence densities that are high in comparison to experiment, a behavior seen previously for many pair potentials, even more specifically for ab initio derived pair potentials.

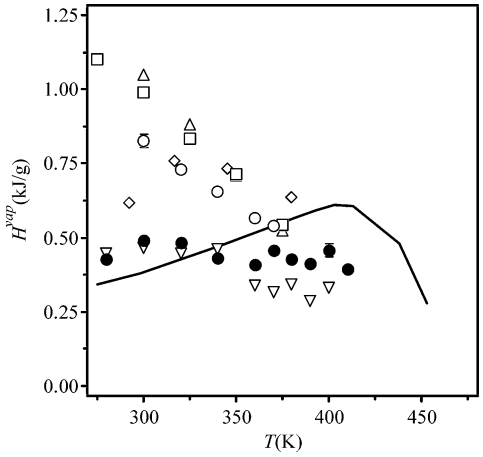

Figure 5. Heat of vaporization, ΔH^{vap}, as calculated from GE simulations (circles) and compared to experiment[41,43,77] (solid line) and models of Figure 2. Symbols are as in Figure 2.

The performance of the TBP model holds up also when examining the vapor pressure, which is displayed in Figure 4. Agreement of the model with experiment is close over the entire temperature range. This outcome is particularly important in demonstrating the ability of the model to describe both low- and high-density phases. For many materials, the vapor pressure is in fact determined exclusively by liquid-phase molecular interactions: the liquid imposes a chemical potential on the vapor, which adopts a pressure to match (in turn this pressure is imposed on the liquid, but has almost no effect on its chemical potential). If the vapor is nearly ideal, then vapor-phase molecular interactions are inconsequential to the vapor pressure. In contrast, for HF the vapor pressure is truly characteristic of molecular interactions in both the liquid and vapor phases, because the vapor is in no way approximately ideal. Molecular models often have difficulty obtaining good agreement with experimental vapor pressures. For water, this has been achieved only by rescaling the potential parameters to force agreement[66,67] or while sacrificing the quality of the characterization of the density.[68] The agreement obtained here by the TBP HF model, accomplished without explicit fitting to the vapor pressure, is a strong indicator of its quality and robustness.

(64) Jedlovszky, P.; Mezei, M.; Vallauri, R. *J. Chem. Phys.* **2001**, *115*, 9883−9894.
(65) Cournoyer, M. E.; Jorgensen, W. L. *Mol. Phys.* **1984**, *51*, 119−132.
(66) Errington, J. R.; Panagiotopoulos, A. Z. *J. Phys. Chem. B* **1998**, *102*, 7470−7475.
(67) Boulougouris, G. C.; Economou, I. G.; Theodorou, D. N. *J. Phys. Chem. B* **1998**, *102*, 1029−1035.
(68) Stillinger, F. H.; Rahman, A. *J. Chem. Phys.* **1974**, *60*, 1545−1557.

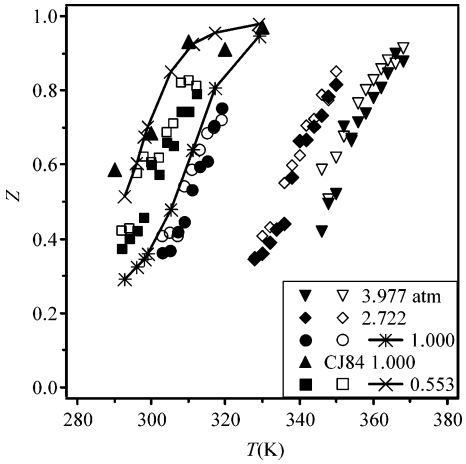

Figure 6. Compressibility factor $Z = P/\rho RT$ for HF in the vapor phase, for isobars at the indicated pressures (in atm). Filled symbols are simulation data for the TBP potential. Open symbols are simulation data for the TBP* potential. Lines joining symbols are experimental data.[39,78] CJ84 indicates data for the Cournoyer−Jorgensen potential.[63,65]

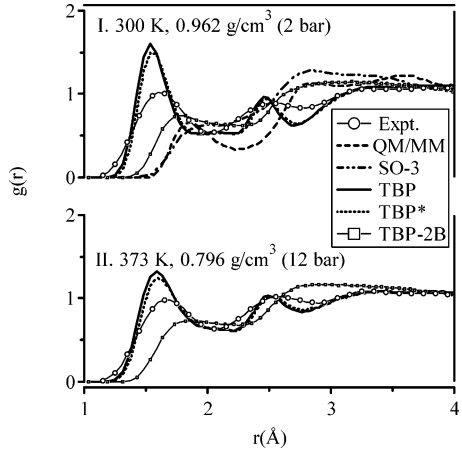

Figure 7. Combined radial distribution function defined in eq 27 as measured in simulations of the several models and compared to experimental data[55] for states I and II of Table 1. TBP is the model proposed here; QM/MM is the $R = 0.973$ model of ref 37, and SO-3 is the model of Klopper et al.[27] studied in ref 36.

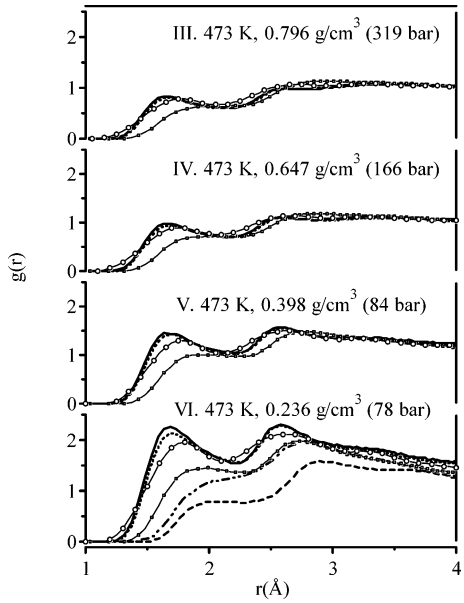

Figure 8. Same as Figure 7, but for states III−VI of Table 1.

The heat of vaporization ΔH^{vap} is presented in Figure 5. The data are a bit noisy, but nevertheless in an important sense they agree with experiment very well. Almost all prior attempts (except for Cournoyer−Jorgensen and Jedlovszky−Vallauri) to describe HF via a molecular model have yielded a heat of vaporization curve that behaves qualitatively like simpler materials, that is, it is zero at the critical temperature and increases monotonically as the temperature is decreased, a behavior seen from TBP-2B. HF instead exhibits a peak in its heat of vaporization, below which ΔH^{vap} decreases with decreasing temperature. Although the present data is mostly flat and the location of a peak in ΔH^{vap} is not distinct, the success of the model in capturing the magnitude of ΔH^{vap} is an attribute to proper treatment of both the liquid and vapor phases.

Equation of State. Liquid-phase and supercritical densities calculated by *NPT* simulation are listed in Table 1, where they are compared to the experimental values[62,64,69] and two other models. Likewise, *NPT*-computed densities for the superheated vapor are presented more completely in Figure 6, where they are given via the compressibility factor $Z = \rho kT$ and compared to experimental data where they are available. Generally, characterization of these densities in Table 1 is where the model performs most poorly. The liquid densities are overestimated by 4−7%, whereas the vapor densities are underestimated by 10−66%, with the comparison being worst at lower densities. The deviation of the supercritical densities from experiment is not surprising and is tied into the lower critical point of the model. The overestimation of the liquid densities is in accord with the VLE findings.

The vapor density of HF is difficult to characterize by a molecular model. Oligomer formation significantly influences the behavior, and the degree to which molecules associate depends very much on a balance between the repulsive part of the potential and the hydrogen-bonding attraction. In other work,[36] we have examined an HF model with various modifications, and have found great sensitivity of the vapor phase properties to these features. It is particularly difficult to get this phase right while still maintaining a good description of the liquid. The performance of the TBP model in capturing the vapor compressibility factor *Z*, shown in Figure 6, surpasses what has been obtained previously with other models, even Cournoyer−Jorgensen. The TBP-2B vapor compressibility factor is calculated and not given here as it is nearly ideal with $Z > 0.9$, indicating the polarization contributes completely to the vapor association.

Structure. The RDFs are shown in Figures 7 and 8 in comparison to experimental data[55] for the states labeled I through VI respectively in Table 1. Figure 7 shows liquid-state conditions for HF, where a notable attribute is seen in the model's ability to locate the radial position of important peaks. The magnitudes of the first set of peaks (up to 3.0 Å) are exaggerated, but the rest of the distribution (between 3.5 and 5.0 Å) agrees favorably with experiment. The first peak corresponds to the intermolecular H−F separation, and its overestimation indicates too-strong hydrogen bonding in the liquid phase. The problem decreases (from state I to II) with increasing temperature and/or decreasing density, and this issue might be connected to the overestimation of the liquid coexist-

(69) Franck, E. U.; Wiegand, G.; Gerhardt, R. *J. Supercrit. Fluid* **1999**, *15*, 127−133.

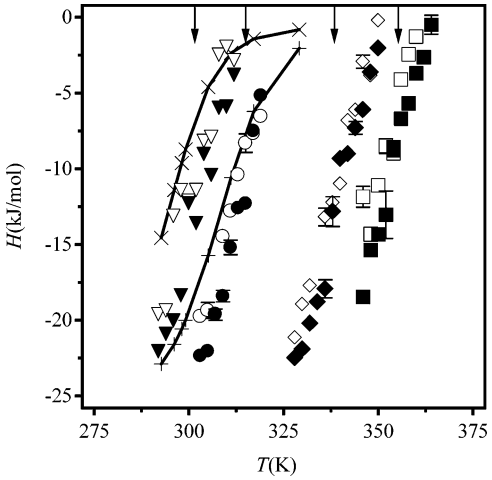

Figure 9. Vapor-phase enthalpy for several isobars. Symbols are as in Figure 6. Experimental data are from Ref 39. Small arrows across top indicate positions of heat-capacity peaks (Figure 10).

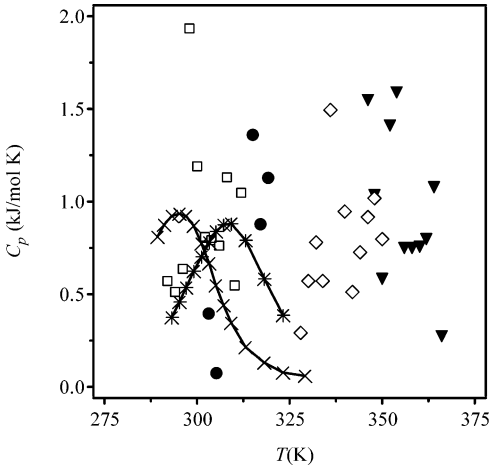

Figure 10. Superheated-vapor heat capacity for several isobars. Symbols are as in Figure 6 except both open and filled markers are for the TBP model without the TBP* model being shown. Experimental data are from Refs 38,39.

ence density observed in the VLE calculations. To the same end, when the liquid RDFs are qualitatively compared to the recent McLain et al.[70] RDF data, the TBP model shows a feature that arises at lower temperatures, a distinct H−H peak. States III−VI in Figure 8 are supercritical. We note that state III is at higher temperature than II, but at the same density, while state VI is near the experimental critical point. The first peaks for the model at these conditions are still too high, but they are much more in line with the experimental data than at states I or II, or than given by the other models. In all cases the radial location of the peaks is described well.

Heat Capacity. Experimentally, the superheated vapor of HF displays a very large peak indicative of a phenomenon having the character of a phase transition (yet the peak is finite, so it is not a true phase change). This behavior is ascribed to a change in the degree of clustering present in the vapor: at high temperatures monomeric species prevail, and as the temperature is lowered at some point there is a rapid increase in population of oligomers. Previous models for HF have failed to capture this behavior adequately. Experimental properties for the superheated vapor are available only at low pressure,[38,39] so the existence of a model that can describe this behavior well would be useful for extrapolating to the unexplored conditions at higher pressure. We examine the TBP model for isobars of 0.553 and 1 atm, respectively, where data are available for comparison to experimental enthalpies and heat capacities. The model is used further to explore two isobars above the available experimental data, specifically 2.722 and 3.997 atm. Simulation and experimental data for enthalpies[39] and heat capacities[38,39] are displayed in Figures 9 and 10, respectively. Data for the TBP-2B model are not present, as shown by Z the behavior is almost ideal. We also record cluster distributions as a function of temperature for the 1 atm isobars, and present these results in Figure 11. The other isobars are also calculated but display similar behavior and are not presented here. The model shows a highly aggregated system at lower temperatures with monomer fractions of 50−60%, increasing monotonically with temperature to 70−90% monomers for the conditions examined here. For this model, linear chain oligomers represent only a small fraction

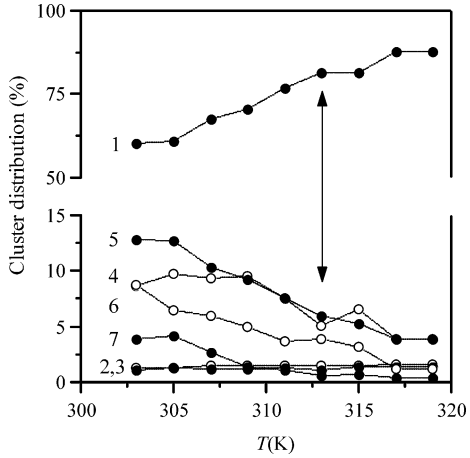

Figure 11. Cluster distribution calculated from simulations for 1.000 atm isobar. Numbers on each line indicate size of cluster; top line describes monomer fraction. Ordinate describes fraction (percent) of all aggregates that are of the indicated size. Arrow indicates temperature of heat-capacity peak (Figure 9) Open markers are cluster with even number of molecules and filled markers are for odd numbers.

(in most cases less than 5%) of the total cluster population, giving way to the more stable ring structure. It is notable that the ring tetramer, pentamer, and hexamer dominate the aggregates and in most case the pentamer is the most prevalent. The finding is a bit interesting considering that most studies of the HF oligomers tend to present the hexamer as the dominant species[38,56,71,72] and other studies speculate that linear chains may dominate over ring structures.[38,73] However, the present results are in accord with more recent experimental data[28,74−76] which have indicated an important, even dominant, role of the pentamer in the vapor. We should also point out that the trimer is not a large component of the vapor, giving some confidence

(70) McLain, S. E.; Benmore, C. J.; Siewenie, J. E.; Molaison, J. J.; Turner, J. F. C. *J. Chem. Phys.* **2004**, *121*, 6448−6455.
(71) Long, R. W.; Hildebrand, J. H.; Morrell, W. E. *J. Am. Chem. Soc.* **1943**, *65*, 182−187.
(72) Spalthoff, W.; Franck, E. U. *Z. Elektrochem.* **1957**, *61*, 993−1000.
(73) Briegleb, G.; Strohmeier, W. *Z. Elektrochem.* **1953**, *57*, 668−674.
(74) Quack, M.; Schmitt, U.; Suhm, M. A. *Chem. Phys. Lett.* **1997**, *269*, 29−38.
(75) Quack, M.; Schmitt, U.; Suhm, M. A. *Chem. Phys. Lett.* **1993**, *208*, 446−452.
(76) Oudejans, L.; Miller, R. E. *J. Chem. Phys.* **2000**, *113*, 971−978.
(77) Kao, C. P. C.; Paulaitis, M. E.; Sweany, G. A.; Yokozeki, M. *Fluid Phase Equil.* **1995**, *108*, 27−46.
(78) Strohmeier, W.; Briegleb, G. *Z. Elektrochem.* **1953**, *57*, 662−667.

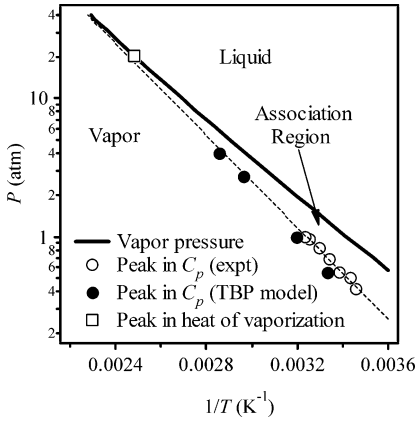

Figure 12. Clausius−Clapeyron plot of saturated vapor pressures. Solid line shows experimental vapor pressures.[39,43,77] Anomalous heat of vaporization peak is designated by the open square at 403 K. Circles depict location of isobaric heat-capacity vs temperature peaks (Figure 9), with open circles describing experimental data[38,39] and filled circles giving results from simulation of the TBP model. Dotted line is a linear extrapolation (ln(*P*) vs 1/*T*) of experimental heat-capacity peak locations into the saturation line. The region between this line and the saturation line is identified as that in which the vapor is most highly associated.

that three-molecule polarization approach did not introduce any anomalous stabilization of the trimer over other oligomers.

Heat capacity data are noisy, as is typical, but peaks are clearly in evidence. In comparison to the available experimental data, the location of the peaks is just a bit too high in temperature, about 2−5 K above experiment. The magnitude of the peaks is hard to compare, as the simulation data are not as smooth as necessary to make a judgment. The peaks persists at higher pressures, where we have no experimental data for comparison.

The connection between the heat capacity peaks and changes in association are evident in all the superheated-vapor plots. Figure 9 indicates the position of the peak temperature for the heat capacity, and in each a glitch is observable in the enthalpy data. It is also clear that a connection exists between the heat capacity peak and cluster distribution. In Figure 11, the heat capacity peak is marked by a noticeable change in the monomer distribution. The effect is perhaps more subtle than expected; the glitch is there, but it does not mark a steep change in the monomer distribution. The change in the monomer distribution may be attenuated by the less obvious reorganization of large oligomers (>3) to smaller dimers and trimers.

Using a simple equilibrium association model, one can surmise that the location of the heat-capacity peak should vary with temperature in the same way as the liquid−vapor saturation pressure, meaning that if presented on a Clausius−Clapeyron plot (ln(*P*) versus 1/*T*), a straight line should be observed. In fact it is particularly interesting to examine this behavior in the context of the vapor−liquid coexistence line, and we do so in Figure 12. Points locating the peak in the heat capacity at different pressures are marked on the plot. The simulation data correspond well with the known experimental data, and the simulation data taken at higher pressure smoothly extend the other points. The region of superheated vapor between the peak heat-capacity line and the coexistence line marks those states in which the "oligomerization transition" has occurred. Interestingly, a linear extrapolation of these points intersects with the coexistence line at about the temperature at which the heat of vaporization goes through its maximum.

Conclusion

The present study addresses mainly the issue of how to treat multi-body energies in simulations in a computationally efficient manner. The methodology diverges from standard polarization techniques by formulating TBP as a true 3-body potential. The methodology is computationally less expensive, removes the need for iterative procedures, and presents possibilities for application of parallelization techniques. In addition, the model is generally derived and may be extended to other hydrogen-bonded systems, including mixtures. The model also shows the capability to be enhanced by comparing to three-body ab initio energies and geometric minima. The key features distinguishing the TBP model from other polarization-based approaches are (1) the use of a trimer-based polarization, taken over all combinations of three molecules (within a cutoff) in the system, and (2) the application of this polarization only in excess of the pairwise polarization.

A comprehensive survey of the TBP model's prediction of experimental properties for HF finds a marked improvement over previous potential models. Good results are obtained for VLE properties, and the structural properties of the liquid and supercritical fluid are satisfactorily reproduced. The unique success of the potential model is its ability to describe the full breadth of properties well over a broad range of state conditions, capturing at least qualitatively all the important anomalies exhibited by the HF system (excluding perhaps its low surface tension, which we did not examine). Nevertheless, HF is a difficult substance to model, and there remains room for improvement in gaining full quantitative correspondence with the experimental behavior.

Success of the model in describing HF indicates that extension to other systems is worthwhile. The most enticing application must be to water. The present model has shown a capability to describe multi-body interactions, introducing polarization without requiring stiffening of the pair repulsion, and thereby gives good structural properties for widely differing state conditions. The same success may be found in the similar hydrogen bonding species of water when applied to popular pair potential models.

Acknowledgment. Financial support was provided by the National Science Foundation, Grant Number CTS-0076515. Computing facilities were provided by the University at Buffalo Center for Computational Research.

JA031877B